Quantifying the Eddy Feedback and the Persistence of the Zonal Index in an Idealized Atmospheric Model

GANG CHEN AND R. ALAN PLUMB

Program in Atmospheres, Oceans and Climate, Massachusetts Institute of Technology, Cambridge, Massachusetts

(Manuscript received 1 April 2009, in final form 12 June 2009)

ABSTRACT

An idealized atmospheric model is employed to quantify the strength of the eddy feedback and the persistence of the zonal index. The strength of the surface frictional damping on the zonal index is varied, and an external zonal momentum forcing is included to compensate for the momentum change associated with the friction change such that the climatological jet latitude and shape are unchanged.

The model can generate a nearly identical climatology and leading mode of the zonal mean zonal wind for different frictional damping rates, except when the jet undergoes a regime transition. For those experiments without a regime transition, as the surface friction is increased, the strength of eddy feedback is enhanced but the zonal index becomes less persistent. A simple feedback model suggests that the *e*-folding decorrelation time scale of the zonal index can be determined by the frictional damping rate and the strength of eddy feedback. The strength of eddy feedback is found to be related to the instantaneous vertical wind shears near the surface controlled by the frictional damping. Furthermore, the climate response to an external zonal torque is proportional to the decorrelation time scale, although the simple prediction used here overestimates the climate response by a factor of 2.

1. Introduction

The zonal index, a measure of the strength of midlatitude westerly winds, characterizes the dominant mode of extratropical zonal winds on intraseasonal to interannual time scales. The spatial pattern associated with the zonal index exhibits an equivalent barotropic dipolar structure in latitude, representing the meridional shift of midlatitude jets (e.g., Nigam 1990; Hartmann and Lo 1998; Lorenz and Hartmann 2001, 2003). The zonal index is essentially the same phenomenon as the annular modes or North Atlantic Oscillation (NAO), defined by the dominant mode of the extratropical geopotential height (Wallace 2000; Vallis et al. 2004; Vallis and Gerber 2008). Simple mechanistic models suggest that the spatial pattern of the zonal index or annular modes can be understood by the global conservation of angular momentum and the momentum transfer by baroclinic eddies (Vallis et al. 2004; Vallis and Gerber 2008).

The temporal pattern of the zonal index is more complex. The observed anomalous zonal winds are often more persistent than baroclinic eddies (e.g., Feldstein and Lee 1998; Hartmann and Lo 1998), and simple and comprehensive general circulation models (GCMs) suggest that the zonal wind persistence is plausibly maintained by a positive eddy feedback that reinforces the anomalous winds (Robinson 1994, 1996; Limpasuvan and Hartmann 2000; Watterson 2002; Gerber and Vallis 2007). More quantitatively, the observed zonal index temporal spectrum can be well described by a red-noise stochastic process (Feldstein 2000a,b), and thus one can quantify the persistence of the zonal index by the *e*-folding time scale of its autocorrelation function (e.g., Gerber et al. 2008b). Furthermore, Lorenz and Hartmann (2001, 2003) showed that the typical decorrelation time scale of the zonal index is greater than the time scale of the frictional damping operating on the zonal index, implicative of a positive eddy feedback.

The zonal index persistence is useful not only to predict the intraseasonal variability of zonal wind in the extratropics but also to quantify the long-term climate response to climate forcing. As is predicted by the fluctuation–dissipation theorem (Leith 1975), the climate response is

Corresponding author address: Gang Chen, Program in Atmospheres, Oceans and Climate, Massachusetts Institute of Technology, Cambridge, MA 02139.
E-mail: gchenpu@mit.edu

DOI: 10.1175/2009JAS3165.1

© 2009 American Meteorological Society

proportional to the projection of the climate forcing onto the dominant mode of climate variability multiplied by the decorrelation time scale of the mode. Recently, Ring and Plumb (2007, 2008) investigated this relation in a simple atmosphere model and found both that the annular mode is the preferred climate response to arbitrary mechanical and thermal forcings and that the response is indeed proportional to the projection of external forcings onto the annular mode. Moreover, Gerber et al. (2008b) found that the Geophysical Fluid Dynamics Laboratory (GFDL) spectral atmospheric dynamical core exhibits different zonal index persistence when the vertical and horizontal resolutions are varied and that the climate response to the same external forcing is larger in the configuration where the zonal index is more persistent. Similarly, Chan and Plumb (2009) found that the tropospheric annular mode response to stratospheric perturbations depends on the persistence of the zonal index in the troposphere. These results may have great implications for climate model projection of future climate change: since the decorrelation time scales of annular modes in the Intergovernmental Panel on Climate Change Fourth Assessment Report (IPCC AR4) models are generally greater than those in the observations, the annular mode–like projection should be taken with caution quantitatively (Gerber et al. 2008a).

However, because of the complicated eddy–mean flow interactions at play it is not well understood what determines the persistence of the zonal index. The propagation of baroclinic eddies and the location of the critical latitude absorption are important to the self-maintenance or the persistence of an eddy-driven jet (Robinson 2006; Gerber and Vallis 2007). As is discussed in Robinson (2000), if the midlatitude eddies are dissipated in the latitudes where they are generated, the resulting eddy heat flux will reduce the meridional temperature gradient in the same latitudes and provide a negative feedback; Conversely, if the eddies propagate away and are absorbed outside the baroclinic zone, the resulting Eliassen–Palm (EP) flux convergence will induce a secondary residual circulation down toward the surface balanced by the friction, which in turn will enhance the meridional temperature gradient in the region of eddy generation and provide a positive feedback. Also, Chen et al. (2008) found that the positive phase of annular modes is accompanied by an increase of eddy phase speed and a poleward shift of the critical latitude of eddy absorption, which may contribute to the positive feedback. Additionally, Son et al. (2008) suggested that the eddy feedback can depend on the barotropic decay of baroclinic eddies that can be affected by the potential vorticity gradient in the subtropics. Despite all these possibilities, little progress has been made in quantifying the decorrelation time of the zonal index with respect to the physical parameters or climatological winds.

Another challenge arises from idealized model studies. Under idealized configurations, the jet stream sometimes switches between a single jet regime and a double jet regime and also persists in each regime for an unrealistically long time (Gerber and Polvani 2009; Chan and Plumb 2009). Also, the change of the dominant mode of zonal wind when the model is perturbed is often accompanied by a change of the climatological wind, making it difficult to understand the causal relationship between the variability and climatology. For instance, Gerber and Vallis (2007) and Son et al. (2008) both found that the decorrelation time scale decreases as the time mean jet moves poleward, but there is not such a relationship as the model resolution is changed (Gerber et al. 2008b).

In this paper, we managed to design some idealized model experiments in which the zonal wind variability can be modified by the strength of the surface friction without affecting the climatological mean wind. The strength of the frictional damping at the surface can influence zonal wind variability in two different ways. On the one hand, stronger frictional damping at the surface can increase anomalous baroclinic wind shears and the associated positive eddy feedback (Robinson 1996, 2000), resulting in more persistent zonal index. On the other hand, as the surface friction is increased, the anomalous barotropic wind is damped more strongly, and thus the zonal index may become less persistent. Despite the complexity, we have successfully related the decorrelation time scale of the zonal index to the frictional damping rate and the strength of eddy feedback, and the latter can be explained by the surface baroclinicity in our model.

We first introduce the model configuration in section 2. In section 3, we show the zonal wind climatology and variability for different frictional damping rates, with a focus on the jet regime transition. We next quantify the eddy feedback and the persistence of the zonal index in section 4 and analyze the mechanism of the feedback in section 5. We explore the relation between the decorrelation time scale of the zonal index and the climate response in section 6. We provide a brief summary and discussion in section 7.

2. Model configuration

We employ the GFDL spectral atmospheric dynamical core and the physical parameterization in Held and Suarez (1994). The temperature field is relaxed to the prescribed zonally symmetric radiative equilibrium temperature, and the wind field is damped by Rayleigh friction

in the planetary boundary layer. The model is run at T42 horizontal resolution with 20 evenly spaced sigma levels. The model is integrated for 4000 days except for one experiment that is run for 8000 days because of the jet regime transition, and the first 400 days of all experiments are discarded. The time mean statistics are computed from daily data independently for each hemisphere and then are averaged over the two hemispheres.

In the frictional parameterization, the strength of friction is maximum at the surface, and the damping rate decreases linearly with the sigma level from its surface value to zero at $\sigma = 0.7$. We refer to the strength of surface friction by its surface damping time scale, and the vertical structure of the friction is kept unchanged in all of our simulations.

We have successfully designed an approach to modify the zonal wind variability and keep the climatological mean wind unchanged. We first apply different frictional damping rates on the zonal mean and eddy components of surface winds. As is shown by Chen et al. (2007), when the damping on the zonal means is reduced, the climatological mean jet moves poleward. To retain the time mean jet at the same latitude, an external momentum forcing is introduced to offset the zonal momentum change associated with the surface friction change. This momentum forcing is time independent, and therefore it does not affect the zonal wind variability directly.

More precisely, the zonally and vertically averaged zonal momentum equation can be written as

$$\frac{\partial\langle\overline{u}\rangle}{\partial t} = \langle\overline{M}\rangle - \langle\overline{F}\rangle, \quad \text{where} \quad \overline{M} = -\frac{1}{a\cos^2\phi}\frac{\partial(\overline{v'u'}\cos^2\phi)}{\partial\phi}. \tag{1}$$

Here overbars denote the zonal means, primes denote the deviations from zonal means, $\langle\ \rangle$ denotes the vertical means, M denotes the eddy momentum flux convergence, F denotes the surface friction, and other symbols follow standard meteorological conventions. For the case of Rayleigh damping, surface drag can be modified as follows:

$$\begin{aligned} F &= \frac{u'}{\tau_{\mathrm{fe}}} + \frac{\overline{u}}{\tau_{\mathrm{fz}}} + \left(\frac{1}{\tau_0} - \frac{1}{\tau_{\mathrm{fz}}}\right)U_0 \\ &= \frac{u'}{\tau_{\mathrm{fe}}} + \left(\frac{\overline{u}}{\tau_{\mathrm{fz}}} - \frac{U_0}{\tau_{\mathrm{fz}}}\right) + \frac{U_0}{\tau_0}, \end{aligned} \tag{2}$$

where τ_{fe} denotes the damping on eddies and τ_{fz} denotes the damping on zonal mean winds. The term $(\tau_0^{-1} - \tau_{\mathrm{fz}}^{-1})U_0$ prescribes the amplitude and structure of external momentum forcing; τ_0 has the same vertical structure as the frictional damping with a surface value of 1.0 day, and U_0 is to be determined. In this paper, we vary the time scale of frictional damping on zonal mean winds τ_{fz} from 0.25 to 1.25 days with an increment of 0.25 day to change the zonal wind variability, while fixing $\tau_{\mathrm{fe}} = 1.0$ day at the surface. The damping rate on the eddies is fixed in all the simulations; therefore, a change of friction does not modify the eddies directly.

To show how this configuration can affect the zonal wind variability and climatology differently, we substitute Eq. (2) into Eq. (1) and obtain the zonal mean momentum equation for the climatological mean

$$\langle[\overline{M}]\rangle - \left(\left\langle\frac{[\overline{u}]}{\tau_{\mathrm{fz}}}\right\rangle - \left\langle\frac{U_0}{\tau_{\mathrm{fz}}}\right\rangle\right) - \left\langle\frac{U_0}{\tau_0}\right\rangle = 0 \tag{3}$$

and for the deviation from climatological mean

$$\frac{\partial\langle\overline{u}^*\rangle}{\partial t} = \langle\overline{M}^*\rangle - \left\langle\frac{\overline{u}^*}{\tau_{\mathrm{fz}}}\right\rangle, \tag{4}$$

where [] denotes the time means and * denotes the deviations from time means.

Our goal is to make the climatological mean wind $[\overline{u}]$ simulated in the model equal to the prescribed U_0. Equation (2) shows that the zonal wind is relaxed to U_0 by a damping rate of τ_{fz}^{-1}, while U_0/τ_0 provides the time-independent zonal momentum source and sink that are required to balance climatological eddy momentum flux convergence. We choose U_0 to be equal to the climatological wind simulated with the standard Held and Suarez (1994) configuration, in which the frictional damping time scales at the surface are set as $\tau_{\mathrm{fe}} = \tau_{\mathrm{fz}} = 1.0$ day. Note that U_0 is a function of both latitudes and sigma levels, but only the lower-level values matter because U_0 is multiplied by the frictional damping coefficients. Although there is no a priori validation that the simulated climatological mean wind should be equal to U_0, our model results show that it holds except for few interesting experiments. Figure 1 shows each component of the climatological zonal momentum balance in Eq. (3) at the latitude of maximum winds for different surface damping rates on the zonal flow. For damping time scales less than 1.0 day, the two terms containing τ_{fz} are exactly canceled out, and therefore the climatological eddy momentum flux is indeed constant. Not surprisingly, the climatological eddy heat flux and eddy kinetic energy are unchanged for these experiments as well (not shown). For the value of 1.25-day drag, the jet can occasionally move to the subtropics and persist for a long time, and the climatological wind is no longer equal to U_0. Therefore, when one varies the damping on the anomalous zonal winds deviating from climatological

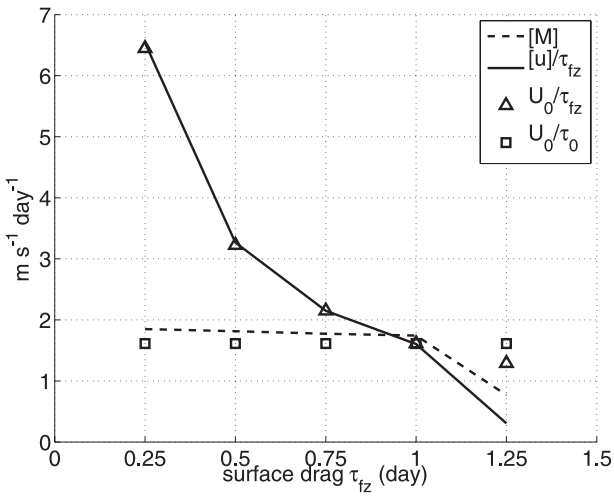

FIG. 1. The time-averaged and zonally and vertically averaged zonal momentum balance at the latitude of maximum winds as the time scale of surface frictional damping on zonal means τ_{fz} is varied. The dashed line, solid line, triangles, and squares represent each term in Eq. (3), respectively. For damping time scales less than 1.0 day, the two terms containing τ_{fz} are exactly canceled out; therefore, although the frictional damping on zonal mean winds is varied, the climatological mean eddy momentum flux is unchanged.

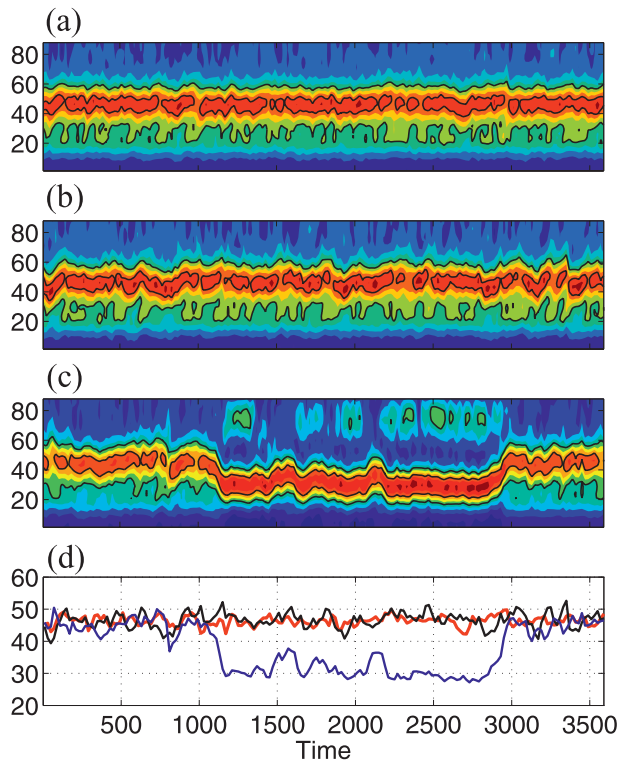

FIG. 2. (a)–(c) The 20-day running mean zonal mean zonal winds at 275 hPa and the corresponding jet latitudes as a function of time. The top three panels are the zonal winds for the (a) 0.5-, (b) 1.0-, and (c) 1.25-day frictional damping, in which the red (blue) shading represents strong (weak) zonal winds, and the black solid lines represent isolines of 15 and 30 m s^{-1}. (d) The corresponding jet latitudes in red, black, and blue for the 0.5-, 1.0-, and 1.25-day drag, respectively.

means, the climatological eddy momentum flux remains unchanged excluding few exceptions. We will examine the jet regime transition intensively in the next section.

3. Zonal wind climatology and variability

Figure 2 shows the 20-day running mean zonal mean zonal winds at 275 hPa and the corresponding jet latitudes as a function of time for the 0.5-day, 1.0-day, and 1.25-day frictional damping on zonal mean winds. The jet latitude is computed by a cubic interpolation for zero meridional shear of zonal mean zonal wind near the jet maximum. For the 0.5- and 1.0-day surface drag, the jet stream wobbles meridionally about its time mean position around 45° latitude, and the meridional shift is larger under weaker frictional damping. For the 1.25-day drag, the jet stream vacillates about 45° latitude for the first 1000 days. During the next 200-day period, the jet moves from about 45° to 30° latitude; simultaneously, a weak subpolar jet appears around 70° latitude. The subtropical and weak subpolar jets continue to coexist for most of the period between days 1200 and 2800 and return to one midlatitude jet regime for the period of days 3000–4000. One additional experiment with 1.5-day drag yields the solution of persistent subtropical and subpolar jets, which is not shown here because the zonal wind is completely different from the prescribed U_0. Briefly speaking, the climatological jet makes the transition from the single jet regime to the double jet regime as the surface friction is reduced; at a critical value of friction, the jet switches between the two jet regimes and persists in each regime for a period much longer than the transitional period. Additionally, the shift of upper-level jets is accompanied by the movement of surface westerly winds in all of our experiments. Despite the seeming artificiality of our perturbation, the jet regime transition and persistence in this model are analogous to those found in many other studies where the width of the baroclinic zone or the model resolution is changed (Lee 1997; Son et al. 2008; Gerber and Polvani 2009; Chan and Plumb 2009).

We further look at the climatological mean jet, the leading mode of the zonal wind, and the probability density function (PDF) of the jet latitude (Fig. 3). The leading mode of zonal wind is defined by the first empirical orthogonal function (EOF) of the zonally and vertically averaged zonal wind, with proper weighting for decreasing area toward to the poles (North et al. 1982). The first EOF explains more than 40% of the total

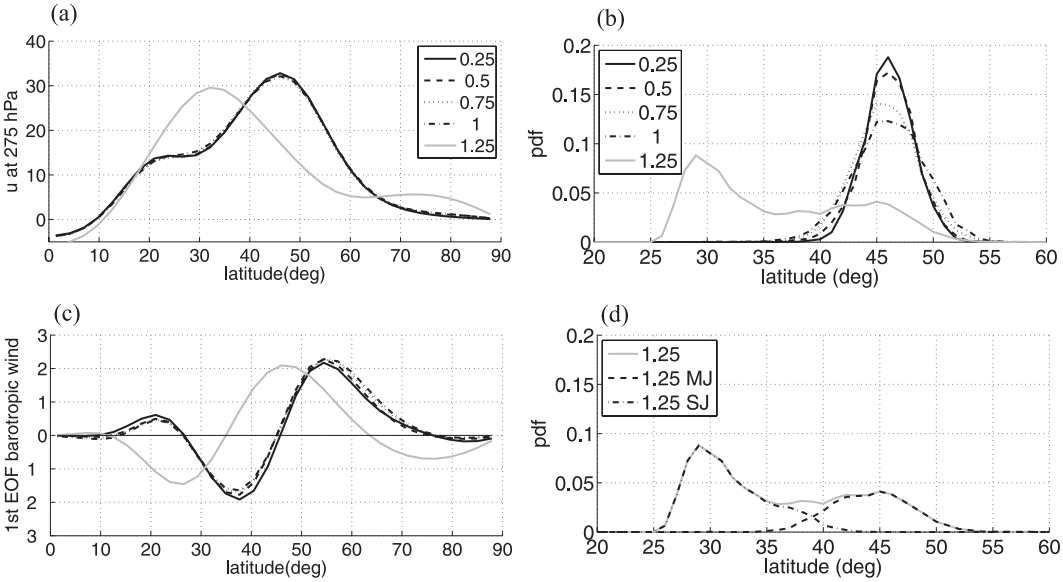

FIG. 3. (a) The time-averaged and zonally averaged zonal wind at 275 hPa. (c) The leading EOF of zonally and vertically averaged zonal wind. The PDF of jet latitude at 275 hPa for (b) different frictional damping time scales and (d) the decomposition of the distribution of the 1.25-day drag into a midlatitude jet (MJ) regime and a subtropical jet (SJ) regime by the latitude of 40° when the regime transition occurs.

variance for all of our experiments. The zonal index is then the principal component associated with the normalized leading EOF. The PDF of jet latitude is constructed from daily data. Since the jet for the 1.25-day surface drag wobbles between two jet regimes, the model is integrated for an additional 4000 days for stability of the PDF.

For the frictional damping time scale from 0.25 to 1.0 days, both the climatological means and the dominant EOFs of zonal wind are nearly identical and center about 45° latitude. The associated jet latitude PDF exhibits a well-defined Gaussian structure, and the peak of the distribution is smaller and the meridional width is slightly broader under weaker frictional damping, suggestive of larger meridional jet vacillations. For the 1.25-day frictional damping, however, the time mean jet is shifted equatorward. The jet latitude PDF reveals a pronounced peak about 30° latitude and a hint of a second peak about 45°. The time series of jet variation can be easily separated into the midlatitude and subtropical jet regimes. (Here we have used the latitude of 40° for the separation when the regime transition occurs.) The portion of the PDF in the midlatitude jet regime shows a Gaussian distribution similar to the PDF of other experiments except that the meridional extent is broader.

Why does a transition of the jet regime occur here? We have been merely reducing the strength of surface frictional damping on zonal mean winds in the model, and the external momentum compensation helps to retain the same climatological jet latitude and shape until the jet regime transition occurs. Because the meridional structure of the jet shift (represented by the leading EOF of zonal wind) is identical, weaker surface drag leads to stronger zonal wind anomalies and larger meridional vacillations; consequently, the jet is more likely to displace to the subtropics. Under the weakest damping, an eddy-driven jet can move to the subtropics and interact with the Hadley cell circulation through the critical layer wave breaking and absorption, which may reinforce the jet persistence in the subtropics, analogous to the self-maintenance of an eddy-driven jet in Robinson (2006). Presumably, the interaction between the Hadley cell and the eddy-driven jet becomes stronger as the two gets closer. Therefore, the regime transition may be accounted for by the distance between the anomalous eddy-driven jet and the Hadley cell. Additionally, we have varied the frictional damping on zonal means for a different profile of U_0 in Eq. (2) where the climatological jet is more poleward. When the friction is reduced, the jet can similarly vacillate in a larger meridional extent and switch to the double jet regime. However, the critical value of the frictional damping time scale for a regime change is larger when the climatological jet is more distant from the subtropics, consistent with the role of the Hadley cell in the regime transition. For the rest of the paper, we will concentrate on the experiments that display no jet regime change.

4. Quantifying the eddy feedback and the persistence of the zonal index

In this section, we quantify the eddy feedback and the persistence of zonal index in the experiments that exhibit no regime change. Following Lorenz and Hartmann (2001), we first project Eq. (4) onto the leading EOFs of zonally and vertically averaged zonal winds that are essentially identical for these experiments in question (Fig. 3c):

$$\frac{\partial z}{\partial t} = m - D^{-1}z, \tag{5}$$

where z is the zonal index, m is the projection of eddy momentum flux convergence, and D is the time scale of the frictional damping acting on the zonal index, which is related to the projection of the zonal and vertical average of surface friction $f = D^{-1}z$.

We have estimated the frictional damping on the zonal index D in three different approaches. First, since the surface friction is directly available from our model, D can be computed through fitting daily data in a least squares way to the linear relationship $z = Df$. Second, Lorenz and Hartmann (2001) computed the observed value of D by examining the cross-spectrum of z and m in the low-frequency range. We can obtain D similarly by using a least squares fit to the linear relationship $z = Dm$, where the 100-day running means of z and m are used to extract the low-frequency variability. Finally, one can even calculate D analytically from the drag coefficient by assuming no vertical variation of zonal wind. The zonal index damping time scale D in various experiments is displayed in Fig. 4 for the three methods, and the methods agree with one another fairly well, indicating that the damping on the zonal index is primarily determined not by the vertical structure of zonal wind but by the strength of surface friction.

Figure 5 shows the autocorrelation functions of the zonal index z and eddy forcing m and their cross correlation for our simulations in the left column. The zonal index decays much slower with lag time than does the eddy forcing, as is the case in observations (e.g., Feldstein and Lee 1998; Lorenz and Hartmann 2001). For the first order of approximation, the autocorrelation function of the zonal index can be approximated by an exponential function, although there exists a noticeable shoulder about the 5-day lag, a hint of which is also seen in the observed NAO index (Ambaum and Hoskins 2002) and other simple models (e.g., Gerber et al. 2008b; Son et al. 2008). A decorrelation time scale τ can be obtained by performing a least squares fit to an exponential function $\exp(-\Delta t/\tau)$ between the autocorrelation value 1 and

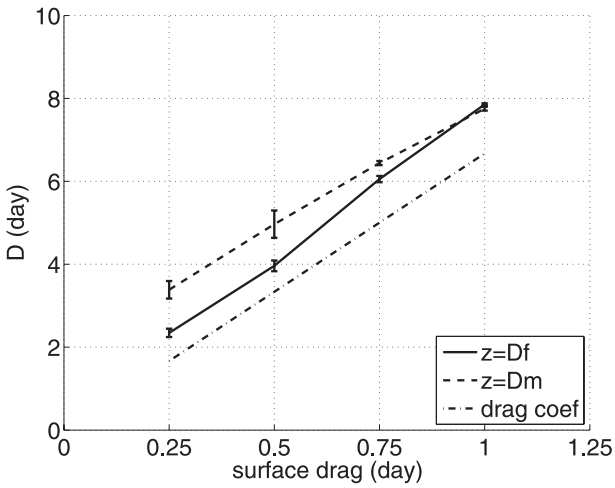

FIG. 4. The time scale of the frictional damping on the zonal index as a function of the damping time scale at the surface, estimated from three approaches described in the text. The error bars denote the difference of the two hemispheres.

$\exp(-1.5)$ [where Δt is the lag time and the threshold value $\exp(-1.5)$ instead of $\exp(-1.0)$ is chosen to minimize the influence of the shoulder]. This decorrelation time describes the zonal wind variability on the time scale longer than the characteristic time of baroclinic eddies. By contrast, the autocorrelation function of the eddy forcing displays a sharp peak with an oscillatory structure at short lags and a long positive tail at large lags. The sharp peak suggests that the eddies have a short decorrelation time, and the long positive tail may be attributable to the modification of the slowly varying zonal flow. This is consistent with the cross correlation of the eddy forcing and the zonal index, which features two maxima in the positive and negative lags and a minimum in between near the zero lag. The eddy forcing is positively correlated with the zonal index in the negative lag where the eddy forcing leads the zonal index, as expected from Eq. (5). In the large positive lag, the positive correlation indicates that the eddies may be modulated by the zonal mean flow.

We quantify the strength of the feedback following a simple model described in Lorenz and Hartmann (2001). The basic assumption is that the eddies have short memory except for those reinforced by the slowly varying eddy-driven zonal winds. The feedback can be parameterized as

$$m = \tilde{m} + Bz, \tag{6}$$

where $\tilde{m}$ denotes the eddy forcing independent of the zonal mean flow and B denotes the strength of the feedback. Substituting Eq. (6) into Eq. (5), we have

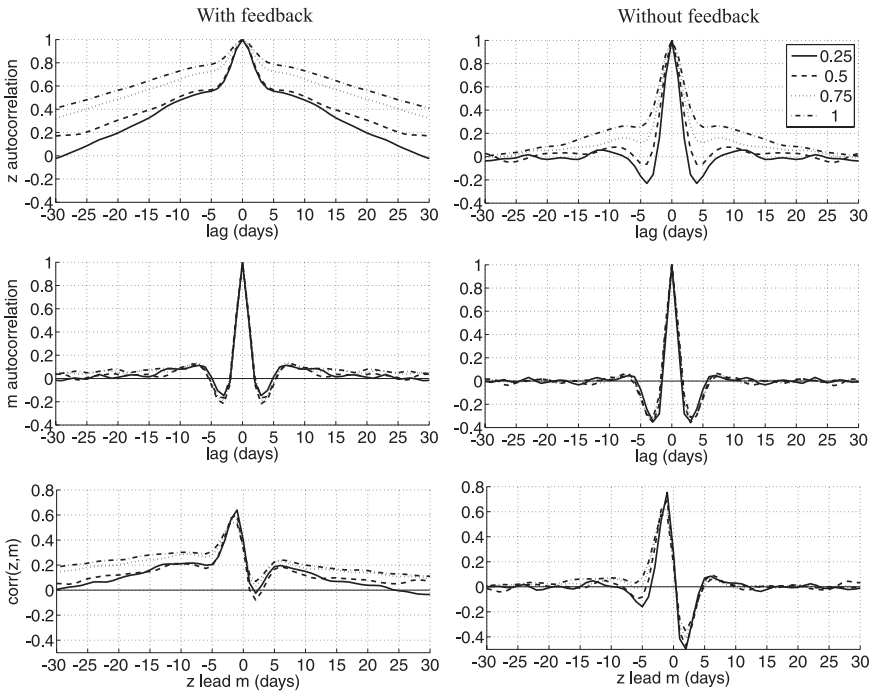

FIG. 5. The autocorrelation functions of (top) the zonal index and (middle) eddy forcing; (bottom) their cross correlations for different surface frictional damping time scales. The left column shows the correlations for z and m, and the right column shows the correlations for $\tilde{z}$ and $\tilde{m}$ where the feedback is eliminated.

$$\frac{\partial z}{\partial t} = \tilde{m} - \tau^{-1} z, \tag{7}$$

$$\tau^{-1} = D^{-1} - B, \tag{8}$$

where τ is the decorrelation time scale of the zonal index, which can be determined by the frictional damping rate D^{-1} minus the strength of the feedback B.

The feedback strength B can be obtained by using the lagged correlation method in Lorenz and Hartmann (2001). Presumably the frictional damping rate is independent of the feedback, and then the zonal index in the absence of the feedback is driven by

$$\frac{\partial \tilde{z}}{\partial t} = \tilde{m} - D^{-1} \tilde{z}. \tag{9}$$

The cross correlation of $\tilde{z}$ and $\tilde{m}$ can be shown to be related to the correlation of z and m. Given the short memory of $\tilde{m}$, the strength of the feedback is the value of B that minimizes the positive cross correlation of $\tilde{z}$ and $\tilde{m}$ when $\tilde{z}$ leads $\tilde{m}$ beyond the typical eddy life time scale. This is derived mathematically and discussed in the appendix. Once the value of B is known, the autocorrelations of $\tilde{z}$ and $\tilde{m}$ without feedback can be obtained in a similar way.

Figure 5 shows that the positive values of the autocorrelations of the zonal index and eddy forcing and their cross correlation at large positive lags are effectively reduced in the absence of the feedback. At a lag larger than the eddy characteristic time, the autocorrelations of z and m and their cross correlation decay roughly as $e^{-\Delta t_L/\tau}$, whereas the autocorrelation of $\tilde{z}$ decays as $e^{-\Delta t_L/D}$ [where Δt_L is the lag time; see also Eqs. (A10) and (A11) in the appendix]; thus, there exist some low-frequency variabilities in the $\tilde{z}$ autocorrelation. By contrast, the correlations at short lags are dominated by impulsive and oscillatory characters of the $\tilde{m}$ autocorrelation. Because the $\tilde{m}$ autocorrelation is almost identical for all of our experiments, its structure can be assumed to be of the form

$$r_{\tilde{m}\tilde{m}}(\Delta t) = \cos(\omega_{\tilde{m}} \Delta t) e^{-|\Delta t|/t_{\tilde{m}}}. \tag{10}$$

The best fit of $r_{\tilde{m}\tilde{m}}(\Delta t)$ to the model results yields $t_{\tilde{m}} = 3.0$ days and $2\pi/\omega_{\tilde{m}} = 7.2$ days. Substituting the best fit into Eq. (A2), we can reproduce the autocorrelation of the zonal index fairly well, including the shoulder around the 5-day lag (Fig. 6). If we remove the sinusoidal part and keep the same $t_{\tilde{m}}$ in Eq. (10), the autocorrelation is flattened at short lags and the shoulder disappears. Similar sensitivity at short lags can be

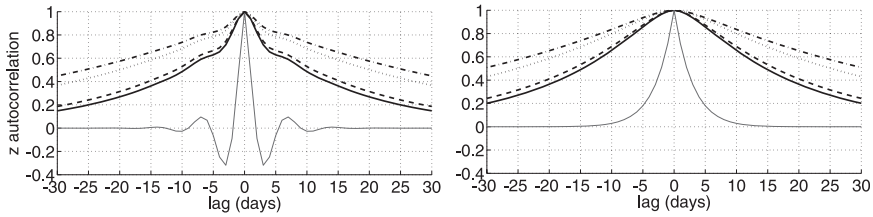

FIG. 6. The autocorrelation function of the zonal index for different surface frictional damping time scales, but the autocorrelation of $\tilde{m}$ is assumed to be of the form of Eq. (10) and is shown in the gray solid line. We use the best fit to the model result on the left, and remove the sinusoidal part and keep the same eddy decorrelation time scale on the right. The lines are as in Fig. 5.

found in the autocorrelation of m and the cross correlation of z and m. This suggests that the shoulder in our simulations is in fact due to the oscillatory nature of the eddy forcing at short lags, which may provide a new insight into the temporal structure of the observed zonal index. The negative value of eddy forcing may be attributed to the negative feedback of eddies in reducing the surface baroclinicity before they propagate away from the source latitude, a process plausibly acting on a short time scale (Robinson 2000).

Figure 7 summarizes the frictional damping on the zonal index, the feedback strength, and the decorrelation time scale of the zonal index as a function of surface friction. Despite a slight overestimate, the decorrelation time scale is predicted fairly well by Eq. (8), showing that the simple feedback model is at work. The simple model explains why the zonal index is more persistent than baroclinic eddies. Although the time scales of the frictional damping and feedback are both less than 10 days, the two processes nearly cancel each other, and the reciprocal of a small residual results in a time scale much larger than either of them. Since both the zonal index damping rate and the feedback strength are approximately proportional to the strength of surface friction, the decorrelation time of the zonal index varies roughly linearly with the surface frictional damping time scale.

It should be noted that if the climatological jet is not retained at the same latitude by the external momentum forcing, the dependence of the decorrelation time scale on surface friction would be more complex. To illustrate this, we remove the external zonal torque by setting $U_0 = 0$ in Eq. (2), and then the westerly jet is allowed to move in latitude. We vary the frictional damping time scale from 0.25 to 1.75 days with an increment of 0.25 day, and the climatological jet gradually moves poleward (Chen et al. 2007). The nodal line of the leading EOF pattern shifts meridionally in accordance with the climatological jet, and therefore the EOF of the respective simulation is used to calculate the projection of zonal wind, eddy momentum flux convergence, and surface friction. We perform the same calculations as in Fig. 7 for the time scale of the zonal index damping, eddy feedback, and the zonal index decorrelation.

Figure 8 shows that our key results still hold in spite of the jet movement in latitude. The strengths of the damping on the zonal index and the eddy feedback are roughly proportional to the strength of surface friction. The simple feedback model predicts the change of the decorrelation time scale fairly well, including the peak around 0.75-day drag. The time scales of the frictional damping and eddy feedback are quite similar in magnitude to their counterparts in Fig. 7, but the change of decorrelation time scale is no longer monotonic. As the frictional damping time increases, the decorrelation time increases from 0.25- to 0.75-day drag and decreases from 0.75- to 1.25-day drag, which is consistent with a slight change in the slope of the eddy feedback B^{-1}. This reconciles the seemingly opposite sensitivity of the decorrelation time scale with respect to the strength of

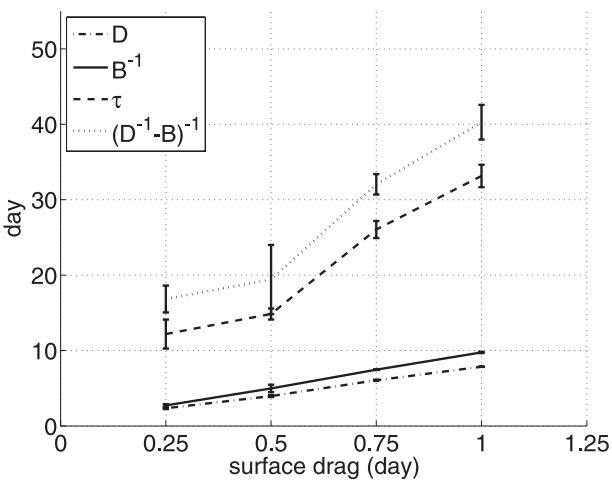

FIG. 7. The time scale of the zonal index damping D, eddy feedback B^{-1}, and the zonal index decorrelation τ as a function of surface friction. The error bars denote the difference of the two hemispheres. Note that the inverse of the eddy feedback is plotted.

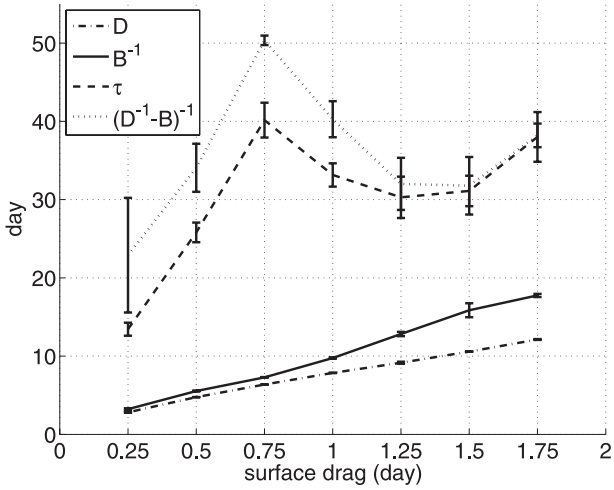

FIG. 8. As in Fig. 7, but the external zonal torque is removed by setting $U_0 = 0$ in Eq. (2). The westerly jet and the leading EOF pattern have shifted in latitude in different experiments, and the leading EOF of the respective simulations are used to calculate the projection of zonal wind, eddy momentum flux convergence, and surface friction. The error bars denote the difference of the two hemispheres. Note that the inverse of the eddy feedback is plotted and that because there is no abrupt jet regime change, the drag is varied in a broader parameter range than in Fig. 7.

surface friction between Ring and Plumb (2007) and Gerber and Vallis (2007). We speculate that the nonmonotonic character here is related to the change in the jet's barotropic and vertical structure as the eddy-driven jet is separated from the subtropical jet [see the top panel of Fig. 2 in Chen et al. (2007)]. The relevant dynamical mechanisms will be explored in the next section.

5. Mechanism of the eddy feedback

Why does the feedback vary roughly linearly with the strength of surface friction? Here we attempt to explain the feedback from the perspective of eddy–mean flow interaction. The eddy momentum flux is controlled by the combination of baroclinic eddy generation at the surface and the meridional wave propagation in the upper troposphere. As the zonal index is increased, it is plausible that the associated meridional wind shear is in favor of equatorward wave propagation and poleward momentum transport, as is parameterized by Eq. (6) with an undetermined feedback parameter B. Meanwhile, the surface baroclinic zone shifts poleward, accompanying anomalous poleward jet movement, and the eddy activity is likely to be generated more vigorously on the climatological jet's poleward side (Robinson 2000; Lorenz and Hartmann 2001).

We explore this baroclinic perspective by comparing the regressions of the zonal mean zonal wind and eddy heat flux with respect to the zonal index in different experiments, as the leading mode of vertically averaged zonal wind has a nearly identical meridional structure. Figure 9 shows the simultaneous regression pattern of zonal mean zonal wind for the 0.5-day and 1.0-day surface drag. In spite of the general similarity of the two regression patterns, they display different vertical wind shears, with a larger shear for stronger surface friction, as expected from the damping effect of surface friction. By the thermal wind relationship, the experiment with stronger surface friction has a stronger meridional temperature gradient near the surface.

Figure 10 displays the lagged regressions of the meridional temperature gradient and eddy heat flux at 875 hPa. We first look at the latitudinal variation with lag time for the 1.0-day drag. Both the temperature gradient and heat flux display an anomalous positive center at 50°–55° and a negative center at 30°–35° over time, in concert with the dipolar structure in the leading mode of zonal wind in Fig. 3. The positive and negative centers at

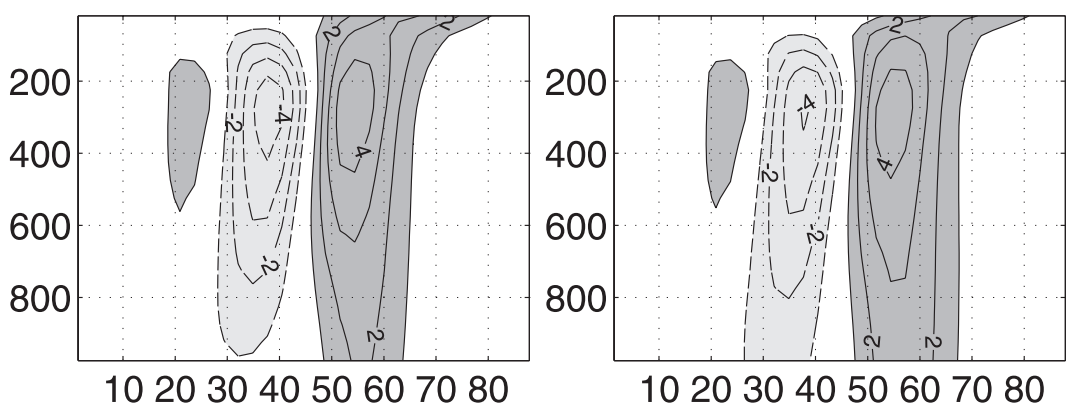

FIG. 9. The regression pattern of zonally averaged zonal wind with respect to the zonal index (defined by the leading mode of vertically averaged zonal wind) for the (left) 0.5-day and (right) 1.0-day drag. The contour interval (CI) is 1 m s^{-1}, and zeros are omitted. The dark (light) shading represents positive (negative) values.

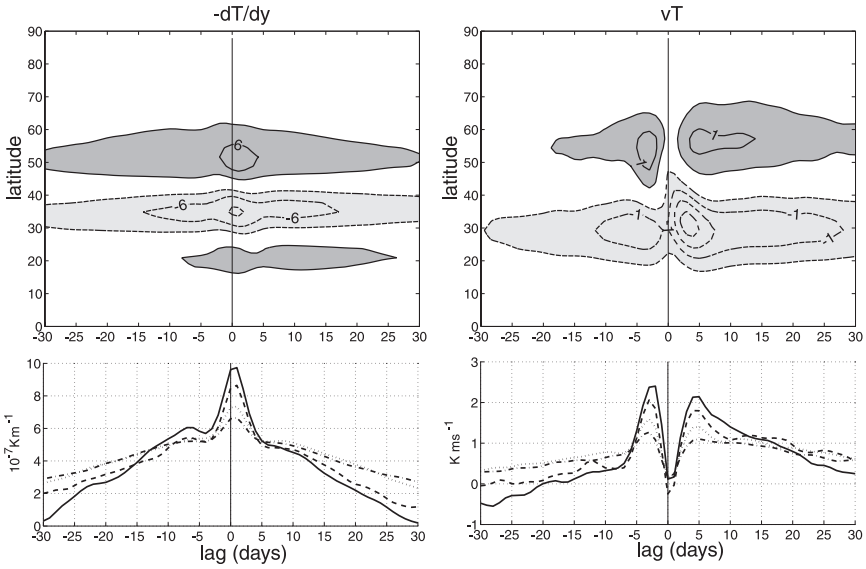

FIG. 10. The lagged regression patterns of (left) the meridional temperature gradient and (right) eddy heat flux at 875 hPa with respect to the zonal index. The top panel shows the regression for the 1.0-day drag as a function of latitude. The contour intervals are 3×10^{-7} K m^{-1} for the temperature gradient and 0.5 K m s^{-1} for the heat flux, and the dark (light) shading represents positive (negative) values. The bottom panel shows the regression at 55° latitude for different damping rates. The lines are as in Fig. 5.

each lag time are of similar magnitude except for the large heat flux anomalies on the jet's equatorward side between the lag day 0 and day 5, which may result from the separation of the eddy-driven jet from the subtropical jet, implicated in the temperature gradient anomalies around 20° latitude. Next, we compare the regressions at 55° latitude on the jet's poleward side for different damping rates; qualitatively similar results are found on the jet's equatorward side. At large lags, the regressions of the temperature gradient and eddy heat flux vary in time as the autocorrelation of the zonal index, consistent with the correlations in Fig. 5. At zero lag, the temperature gradient is greater for larger surface frictional damping. The heat flux displays a minimum at the zero lag, and the amplitude of heat flux within the 5-day lag increases in accordance with the temperature gradient at zero lag. This corroborates the baroclinic mechanism that the enhanced baroclinicity near the surface under stronger frictional damping generates more baroclinic waves, which can in turn reinforce the anomalous zonal index.

In summary, the regression analysis shows that the increased eddy feedback with the strength of surface friction in our model can be explained by the increased anomalous vertical wind shears near the surface controlled by friction. The feedback parameter B is plausibly dependent on the lower-level baroclinicity that controls the growth rate of baroclinic eddies. Nevertheless, since these experiments have nearly identical meridional wind shears, our results cannot exclude the possible control of barotropic shears on baroclinic instability (James 1987) and the eddy feedback (Gerber and Vallis 2007). When the jet is allowed to move meridionally, the barotropic control can play an additional role with regard to the baroclinic mechanism. The change in the jet's barotropic structure may explain the change in the slope of the feedback parameter in Fig. 8 and thus the nonmonotonic behavior of the decorrelation time. This barotropic control may have been incorporated when different EOF patterns were used to compute the projections; however, a more careful analysis is beyond the scope of our study.

6. Relation of the decorrelation time scale and climate response

Because the decorrelation time scale of the zonal index varies with the surface friction, this provides an ideal set of experiments to test the relationship between the decorrelation time and climate response. We imposed an artificial zonal torque in each experiment as described in Chen and Zurita-Gotor (2008). As is shown by Ring and Plumb (2007), the climate response is proportional to the projection of an external torque onto the modes independent of the forcing location. The torque is chosen to be centered at 50° latitude and σ = 0.85, with a Gaussian latitudinal structure of half-width

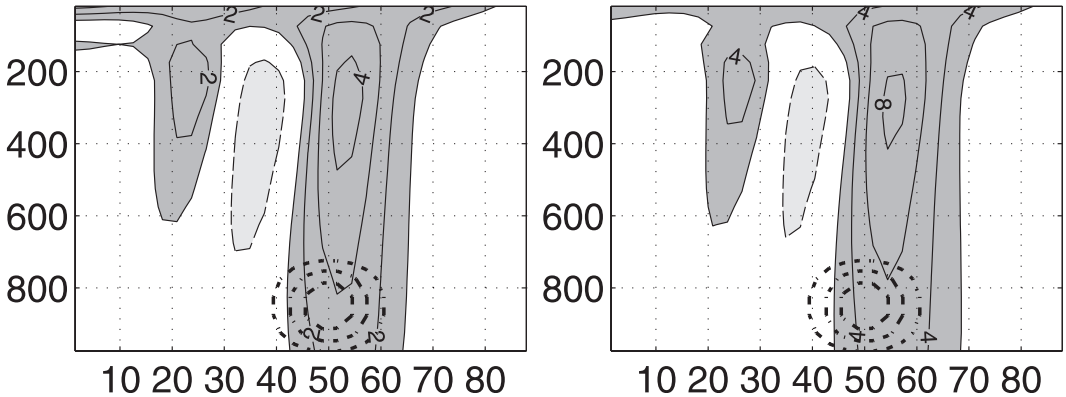

FIG. 11. The zonally averaged zonal wind response to an external zonal torque for the (left) 0.5-day and (right) 1.0-day drag. The torque is prescribed in the lower troposphere, shown by the dashed contours with a maximum acceleration of 4 m s^{-1} day^{-1}. The CIs of zonal wind change are 1 m s^{-1} for 0.5-day drag and 2 m s^{-1} for 1.0-day drag; zeros are omitted. The dark (light) shading represents positive (negative) values.

9°, and a sinusoidal vertical structure only in the lower troposphere $\cos[(\sigma - 0.85)\pi/0.3]$, $0.7 < \sigma < 1.0$. The maximum zonal wind acceleration is set as 4 m s^{-1} day^{-1} in half of the experiments. In the other half of experiments, the acceleration is prescribed as 2 m s^{-1} day^{-1} for those with large decorrelation times (0.75- and 1.0-day drag) and as 8 m s^{-1} day^{-1} for those with small decorrelation times (0.25- and 0.5-day drag). The response is adjusted by a factor of 2 for comparison with the 4 m s^{-1} day^{-1} experiments in order to justify the linearity of the response with the forcing amplitude.

Figure 11 shows the zonal wind response to the external zonal torque for the 0.5- and 1.0-day drag. Although the positive center of zonal wind change at about 55° is greater than the negative center at 35°, in contrast to the dipolar pattern in the leading mode of zonal wind (Fig. 9), the patterns of zonal wind change resemble each other remarkably and project largely onto the leading mode of zonal wind. The amplitude of zonal wind change is about twice as strong in the 1.0-day drag. Recalling that the decorrelation time scale in this experiment is of a factor of 2 larger, this is consistent with the fluctuation–dissipation theorem.

We further probe a quantitative relationship between the decorrelation time scale and climate response. A simple relation can be obtained from Eq. (7) for a small external zonal torque, since both the random eddy forcing and the time derivative of the zonal index vanish in the time mean:

$$\Delta z \approx \tau \times \Gamma, \tag{11}$$

where Γ is the projection of the external zonal torque onto the leading mode of zonal wind and Δz is the climate response in the mode. In comparison with Leith (1975), we have only employed the zonally and vertically averaged zonal wind and its dominant EOF mode.

Figure 12 shows that the zonal wind response is linear with respect to the forcing amplitude, since the adjusted responses for the same decorrelation time are almost equal. Moreover, the climate response to the same forcing increases approximately linearly with the decorrelation time scale. However, the model response is about half of the value predicted by the decorrelation time scale times the external forcing. A similar overestimate by a factor of 2 is also seen in Ring and Plumb (2007, 2008) and Gerber et al. (2008b) for the annular mode–like response to an external torque. Despite the quantitative limitation due to our oversimplification to the fluctuation dissipation theorem, the simple relationship provides a useful tool to understand and quantify the annular mode–like climate response with respect to climate forcing.

7. Summary and discussion

We have used an idealized atmospheric model to examine what determines the strength of the eddy feedback and the persistence of the zonal index. The strength of the surface frictional damping on the zonal index is varied, and an external zonal momentum forcing is included to compensate for the momentum change associated with the friction change in order to keep the climatological jet latitude and shape.

The model can generate a nearly identical climatology and leading mode of the zonal mean zonal wind for different frictional damping rates, except when the jet undergoes a regime transition. As the surface friction is increased, the strength of eddy feedback is enhanced but the zonal index becomes less persistent. A simple feedback

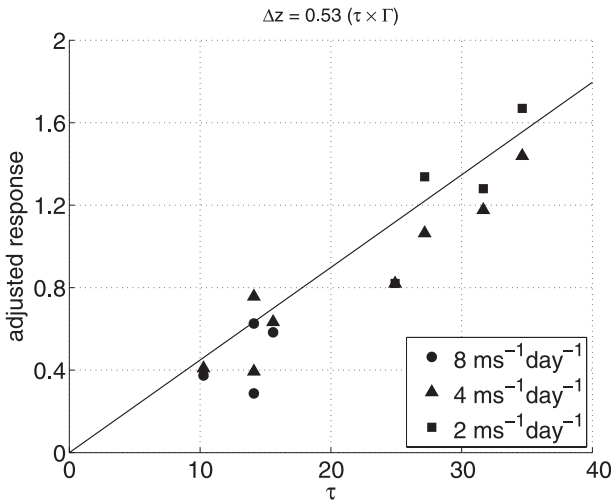

FIG. 12. The relation between the decorrelation time scale and the zonal wind response projected onto the leading mode of zonal wind. The maximum zonal wind acceleration is set as 4 m s^{-1} day^{-1} in half of the experiments. In the other half of experiments, the acceleration is prescribed as 2 m s^{-1} day^{-1} for those with large decorrelation times (0.75- and 1.0-day drag) and 8 m s^{-1} day^{-1} for those with small decorrelation times (0.25- and 0.5-day drag). The response is adjusted by a factor of 2 for comparison with the 4 m s^{-1} day^{-1} experiments in order to justify the linearity of the response with the forcing amplitude.

model suggests that the *e*-folding decorrelation time scale of the zonal index can be determined by the frictional damping rate and the strength of eddy feedback. The strength of the eddy feedback is found to be related to the instantaneous vertical wind shears near the surface, which are controlled by the frictional damping. Accordingly, the lagged regression with respect to the zonal index shows that the eddy heat flux in short positive lags corresponds roughly linearly to the magnitude of surface meridional temperature gradient at the zero lag. Furthermore, the climate response to an external zonal torque is found to be proportional to the decorrelation time scale of the unforced zonal index variability, although our simple prediction overestimates the climate response by a factor of 2.

This simple model of quantifying the persistence of the zonal index can still hold in the presence of the jet movement, although a complete understanding of eddy feedback would need to consider the control of barotropic flow on baroclinic instability (James 1987) in addition to this baroclinic mechanism. Therefore, this simple model is of value to understand the zonal index variability in more realistic situations. The stratosphere–troposphere coupling can increase the persistence of zonal index in the troposphere through the downward propagation of zonal wind anomalies (Baldwin et al. 2003). Recently, Gerber and Vallis (2007) and Son et al. (2008) found that the presence of topography can reduce the persistence of the zonal index and argued that a mountain can block the zonal propagation of baroclinic waves, reducing the eddy feedback on the zonal index. Our simple model, together with theories of planetary wave propagation forced by surface topography or refracted in the lower stratosphere, may help to quantify the role of eddy feedback and planetary wave propagation in the observed or modeled annular mode variability.

Acknowledgments. GC is supported by the NOAA Climate and Global Change Postdoctoral Fellowship, administered by the University Corporation for Atmospheric Research. RAP is supported by the National Science Foundation through Grant ATM-0808831. We thank two anonymous reviewers for constructive comments that improved our paper greatly, especially for the comments on the potential role of the jet movement in the eddy feedback.

APPENDIX

The Covariance

The covariance of a and b at the lag time Δt is denoted as

$$C_{ab}(\Delta t) = \mathrm{Cov}\{a(t),\ b(t+\Delta t)\}.$$

The solution of Eq. (7) can be written as

$$z(t) = \int_{-\infty}^{0} \tilde{m}(s+t)e^{s/\tau}\, ds. \tag{A1}$$

Then the autocovariance of z and the covariance of z and $\tilde{m}$ are

$$C_{zz}(\Delta t) = \int_{-\infty}^{0}\int_{-\infty}^{0} C_{\tilde{m}\tilde{m}}(\Delta t + r - s)e^{(r+s)/\tau}\, ds\, dr, \tag{A2}$$

$$C_{z\tilde{m}}(\Delta t) = \int_{-\infty}^{0} C_{\tilde{m}\tilde{m}}(\Delta t - s)e^{s/\tau}\, ds. \tag{A3}$$

Using Eq. (6), the autocovariance of m and the covariance of z and m are

$$\begin{aligned} C_{mm}(\Delta t) &= \mathrm{Cov}\{\tilde{m}(t) + Bz(t),\ \tilde{m}(t+\Delta t) + Bz(t+\Delta t)\} \\ &= C_{\tilde{m}\tilde{m}}(\Delta t) + B\{C_{z\tilde{m}}(\Delta t) + C_{z\tilde{m}}(-\Delta t)\} \\ &\quad + B^2 C_{zz}(\Delta t), \end{aligned} \tag{A4}$$

$$\begin{aligned} C_{zm}(\Delta t) &= \mathrm{Cov}\{z(t),\ \tilde{m}(t+\Delta t) + Bz(t+\Delta t)\} \\ &= C_{z\tilde{m}}(\Delta t) + BC_{zz}(\Delta t). \end{aligned} \tag{A5}$$

We are interested in the covariance at large lag $\Delta t_L \gg t_{\tilde{m}}$, where $t_{\tilde{m}}$ is the decorrelation time scale of $\tilde{m}$ and the autocovariance of $\tilde{m}$ satisfies

$$C_{\tilde{m}\tilde{m}}(\pm\Delta t_L) = 0. \tag{A6}$$

Using the approximation $C_{\tilde{m}\tilde{m}}(\pm\Delta t_L) \simeq 0(\Delta t_L > 3t_{\tilde{m}})$, a change of variable to Eq. (A2) and (A3) yields

$$C_{zz}(\Delta t_L) \simeq \frac{\tau}{2} e^{-\Delta t_L/\tau} \int_{-3t_{\tilde{m}}}^{3t_{\tilde{m}}} C_{\tilde{m}\tilde{m}}(x) e^{x/\tau}\, dx, \tag{A7}$$

$$C_{z\tilde{m}}(\Delta t_L) \simeq 0, \tag{A8}$$

$$C_{z\tilde{m}}(-\Delta t_L) \simeq e^{-\Delta t_L/\tau} \int_{-3t_{\tilde{m}}}^{3t_{\tilde{m}}} C_{\tilde{m}\tilde{m}}(x) e^{x/\tau}\, dx, \tag{A9}$$

where we have used the fact that $\tilde{m}$ decorrelates more quickly than $z(t_{\tilde{m}} \ll \tau)$.

Substituting into Eq. (A4) and (A5), the autocovariance and cross-covariance functions vary at large lags as

$$\begin{aligned} &C_{zz}(\Delta t_L), \quad C_{zm}(-\Delta t_L) \sim e^{-\Delta t_L/\tau} \\ &C_{mm}(\Delta t_L), \quad C_{zm}(\Delta t_L) \sim B e^{-\Delta t_L/\tau}. \end{aligned} \tag{A10}$$

Here we have assumed that the feedback strength B is small.

From Eq. (10), one can also obtain that the covariance functions without the feedback vary at large lags as

$$\begin{aligned} C_{\tilde{z}\tilde{z}}(\Delta t_L), \quad C_{\tilde{z}\tilde{m}}(-\Delta t_L) &\propto e^{-\Delta t_L/D} \\ C_{\tilde{z}\tilde{m}}(\Delta t_L) &\simeq 0. \end{aligned} \tag{A11}$$

Lorenz and Hartmann (2001) derived the relation between the covariance functions $C(\Delta t)$ and the covariances without the feedback $C_{\sim}(\Delta t)$ in their appendix C [note that our notation replaces the symbols (τ, b, σ) in their paper by (D, B, τ)]:

$$\begin{aligned} C_{\sim}(\Delta t) = C(\Delta t) - B\left(1 - \frac{BD}{2}\right) \\ \times \int_{-\infty}^{\infty} \exp\left(\frac{-|\Delta t - s|}{D}\right) C(s)\, ds. \end{aligned} \tag{A12}$$

Here $C_{\sim}(\Delta t)$ can be any of the covariance functions $C_{\tilde{z}\tilde{m}}(\Delta t)$, $C_{\tilde{z}\tilde{z}}(\Delta t)$ and $C_{\tilde{m}\tilde{m}}(\Delta t)$, and $C(\Delta t)$ denotes the corresponding covariance $C_{zm}(\Delta t)$, $C_{zz}(\Delta t)$, or $C_{mm}(\Delta t)$; B is a free parameter that can be determined by the constraint of $C_{\tilde{m}\tilde{m}}(\Delta t_L) \simeq 0$ or $C_{\tilde{z}\tilde{m}}(\Delta t_L) \simeq 0$. The latter is chosen because the cross correlation of z and m at large positive lags deviates from zero more than does the autocorrelation of m (Fig. 5). In practice, B is found by minimizing the deviation of $C_{\tilde{z}\tilde{m}}(\Delta t)$ from zero for the time lag $\Delta t > 10$ days. The correlation functions are calculated from the covariances by $r_{ab}(\Delta t) = C_{ab}(\Delta t)/[C_{aa}^{1/2}(\Delta t) C_{bb}^{1/2}(\Delta t)]$.

REFERENCES

Ambaum, M., and B. Hoskins, 2002: The NAO troposphere–stratosphere connection. *J. Climate,* **15,** 1959–1978.

Baldwin, M. P., D. B. Stephenson, D. W. J. Thompson, T. J. Dunkerton, A. J. Charlton, and A. O'Neill, 2003: Stratospheric memory and skill of extended-range weather forecasts. *Science,* **301,** 636–640.

Chan, C. J., and R. A. Plumb, 2009: The response to stratospheric forcing and its dependence on the state of the troposphere. *J. Atmos. Sci.,* **66,** 2107–2115.

Chen, G., and P. Zurita-Gotor, 2008: The tropospheric jet response to prescribed zonal forcing in an idealized atmospheric model. *J. Atmos. Sci.,* **65,** 2254–2271.

——, I. M. Held, and W. A. Robinson, 2007: Sensitivity of the latitude of the surface westerlies to surface friction. *J. Atmos. Sci.,* **64,** 2899–2915.

——, J. Lu, and D. Frierson, 2008: Phase speed spectra and the latitude of surface westerlies: Interannual variability and global warming trend. *J. Climate,* **21,** 5942–5959.

Feldstein, S., 2000a: Is interannual zonal mean flow variability simply climate noise? *J. Climate,* **13,** 2356–2362.

——, 2000b: The timescale, power spectra, and climate noise properties of teleconnection patterns. *J. Climate,* **13,** 4430–4440.

——, and S. Lee, 1998: Is the atmospheric zonal index driven by an eddy feedback? *J. Atmos. Sci.,* **55,** 3077–3086.

Gerber, E. P., and G. K. Vallis, 2007: Eddy–zonal flow interactions and the persistence of the zonal index. *J. Atmos. Sci.,* **64,** 3296–3311.

——, and L. M. Polvani, 2009: Stratosphere–troposphere coupling in a relatively simple AGCM: The importance of stratospheric variability. *J. Climate,* **22,** 1920–1933.

——, ——, and D. Ancukiewicz, 2008a: Annular mode time scales in the Intergovernmental Panel on Climate Change Fourth Assessment Report models. *Geophys. Res. Lett.,* **35,** L22707, doi:10.1029/2008GL035712.

——, S. Voronin, and L. M. Polvani, 2008b: Testing the annular mode autocorrelation timescale in simple atmospheric general circulation models. *Mon. Wea. Rev.,* **136,** 1523–1536.

Hartmann, D. L., and F. Lo, 1998: Wave-driven zonal flow vacillation in the Southern Hemisphere. *J. Atmos. Sci.,* **55,** 1303–1315.

Held, I. M., and M. J. Suarez, 1994: A proposal for the intercomparison of the dynamical cores of atmospheric general circulation models. *Bull. Amer. Meteor. Soc.,* **75,** 1825–1830.

James, I. N., 1987: Suppression of baroclinic instability in horizontally sheared flows. *J. Atmos. Sci.,* **44,** 3710–3720.

Lee, S., 1997: Maintenance of multiple jets in a baroclinic flow. *J. Atmos. Sci.,* **54,** 1726–1738.

Leith, C. E., 1975: Climate response and fluctuation dissipation. *J. Atmos. Sci.,* **32,** 2022–2026.

Limpasuvan, V., and D. L. Hartmann, 2000: Wave-maintained annular modes of climate variability. *J. Climate,* **13,** 4414–4429.

Lorenz, D. J., and D. L. Hartmann, 2001: Eddy–zonal flow feedback in the Southern Hemisphere. *J. Atmos. Sci.,* **58,** 3312–3327.

——, and ——, 2003: Eddy–zonal flow feedback in the Northern Hemisphere winter. *J. Climate,* **16,** 1212–1227.

Nigam, S., 1990: On the structure of variability of the observed tropospheric and stratospheric zonal-mean wind. *J. Atmos. Sci.,* **47,** 1799–1813.

North, G. R., T. L. Bell, R. F. Cahalan, and F. J. Moeng, 1982: Sampling errors in the estimation of empirical orthogonal functions. *Mon. Wea. Rev.,* **110,** 699–706.

Ring, M. J., and R. A. Plumb, 2007: Forced annular mode patterns in a simple atmospheric general circulation model. *J. Atmos. Sci.,* **64,** 3611–3626.

——, and ——, 2008: The response of a simplified GCM to axisymmetric forcings: Applicability of the fluctuation–dissipation theorem. *J. Atmos. Sci.,* **65,** 3880–3898.

Robinson, W. A., 1994: Eddy feedbacks on the zonal index and eddy–zonal flow interactions induced by zonal flow transience. *J. Atmos. Sci.,* **51,** 2553–2562.

——, 1996: Does eddy feedback sustain variability in the zonal index? *J. Atmos. Sci.,* **53,** 3556–3569.

——, 2000: A baroclinic mechanism for the eddy feedback on the zonal index. *J. Atmos. Sci.,* **57,** 415–422.

——, 2006: On the self-maintenance of midlatitude jets. *J. Atmos. Sci.,* **63,** 2109–2122.

Son, S. W., S. Lee, S. B. Fledstein, and J. E. Ten Hoeve, 2008: Time scale and feedback of zonal mean flow variability. *J. Atmos. Sci.,* **65,** 935–952.

Vallis, G. K., and E. P. Gerber, 2008: Local and hemispheric dynamics of the North Atlantic Oscillation, annular patterns and the zonal index. *Dyn. Atmos. Oceans,* **44,** 184–212.

——, ——, P. J. Kushner, and B. A. Cash, 2004: A mechanism and simple dynamical model of the North Atlantic Oscillation and annular modes. *J. Atmos. Sci.,* **61,** 264–280.

Wallace, J. M., 2000: North Atlantic Oscillation/Annular Mode: Two paradigms—one phenomenon. *Quart. J. Roy. Meteor. Soc.,* **126,** 791–805.

Watterson, I. G., 2002: Wave–mean flow feedback and the persistence of simulated zonal flow vacillation. *J. Atmos. Sci.,* **59,** 1274–1288.